International Journal of Thermophysics, Vol. 21, No. 5, 2000

A Thermodynamic Property Model for Fluid-Phase Propane

H. Miyamoto[1, 2] and K. Watanabe[1]

Received April 26, 2000

A fundamental equation of state for propane (R-290), formulated in terms of the non-dimensional Helmholtz free energy, is presented. It was developed based on selected reliable measurements for pressure-volume-temperature (PVT), isochoric and isobaric heat capacities, speed of sound, and the saturation properties which were all converted to ITS-90. Supplementary input data calculated from a virial equation for the vapor-phase PVT properties at lower temperatures and other correlations for the saturated vapor pressures and saturated vapor- and liquid-densities have also been used. The present equation of state includes 19 terms in the residual part and represents most of the reliable experimental data accurately in the range of validity from 85.48 K (the triple point temperature) to 623 K, at pressures to 103 MPa, and at densities to 741 $kg \cdot m^{-3}$. The smooth behavior of the derived thermodynamic properties in the entire fluid phase is demonstrated. In addition, graphical and statistical comparisons between experimental data and the available thermodynamic models, including the present one, showed that the present model can provide a physically sound representation of all the thermodynamic properties of engineering importance.

KEY WORDS: equation of state; Helmholtz free energy; hydrocarbon; natural working fluid; propane; R-290; refrigerant; thermodynamic property.

1. INTRODUCTION

Hydrofluorocarbon (HFC) refrigerants and their binary and/or ternary mixtures are being considered as appropriate alternatives to replace hydrochlorofluorocarbon (HCFC) refrigerants, such as R-22 which has been used almost exclusively for air-conditioning equipment worldwide. If we desire a long-term alternative refrigerant without any impact on the global

[1] Department of System Design Engineering, Faculty of Science and Technology, Keio University, 3-14-1, Hiyoshi, Kohoku-ku, Yokohama 223-8522, Japan.
[2] To whom correspondence should be addressed.

0195-928X/00/0900-1045$18.00/0

environment, however, it has been suggested that some hydrocarbons which have no impact both on the stratospheric ozone depletion and global warming should be used.

Among such candidates, the so-called natural refrigerants including hydrocarbons, carbon dioxide, and water, propane (R-290) is proposed as one of the most essential substances in several promising mixtures, although its flammability has to be reduced, for example, by blending it with non-flammable HFC refrigerants, such as R-134a or R-125. Alternatively, hydrocarbon mixtures including propane + isobutane (R-600a) blends may also be promising if advanced technology becomes available to solve the flammability issue in the near future.

With this background in mind, we aimed to develop an accurate thermodynamic property model for the fluid phase of propane with new thermodynamic property data that have recently become available for R-290. It is also part of our objectives to improve the existing formulations, some of which were developed nearly two decades ago.

A Helmholtz free energy function was used to formulate an accurate equation of state, which has been proven effective for the modeling of HFC refrigerants. From the 3100 thermodynamic property data collected, we selected several sets of reliable measurements as a set of "input data." Three sets of supplementary input data from ancillary correlations regarding the saturated vapor-pressures and saturated vapor- and liquid-densities were also prepared. In addition, we used a set of supplementary gaseous PVT data as input data at lower temperatures on the basis of a truncated virial equation of state. The Helmholtz free energy model developed here represents most of the experimental data within the given uncertainty, and the range of validity of the model covers temperatures from 85.48 K (the triple point temperature given by Goodwin and Haynes [1] converted to ITS-90) to 623 K, pressures up to 103 MPa, and densities up to 741 $kg \cdot m^{-3}$. The programs for regressing the experimental data were developed by Tillner-Roth [2] for the formulations of HFC refrigerants and their mixtures (published by Tillner-Roth et al. [3, 4]).

2. SELECTION OF INPUT DATA

2.1. Data Survey

We collected about 3100 experimental thermodynamic property measurements for R-290. A summary of the data in the single-phase region such as PVT, caloric and acoustic property measurements is listed in Table I, and the saturation property data including vapor pressures, vapor- and liquid-densities, liquid heat capacities, and speeds of sound are summarized

Table I. Single-Phase Experimental Data for R-290

First author[a]	Ref.	Property	Phase	No. of data	P Range (MPa)	P δP^b (%)	ρ Range ($kg \cdot m^{-3}$)	ρ $\delta\rho$ (%)	T Range (K)	T δT^b (mK)
Reamer	5	PVT	Vapor	139	0.1–16	0.05	1–218	0.2	311–511	n.a.
Dawson	6	PVT	Vapor	18	0.05–0.1	n.a.	1–3	n.a.	243–348	n.a.
Warowny	7	PVT	Vapor	51	0.3–6.4	0.02	5–170	n.a.	373–423	10
Thomas#	8	PVT	Vapor	322	1.6–22	0.003(0.01)	35–216	n.a.	323–623	1
Straty#	9	PVT	Vapor	85	0.2–21	0.015	2–216	0.1	373–598	n.a.
Reamer	5	PVT	Liquid	167	1.4–69	0.05	224–576	0.2	311–511	n.a.
Dittmer#	10	PVT	Liquid	336	1.0–103	0.6	320–590	0.1	273–413	100
Ely#	11	PVT	Liquid	222	0.3–43	80 Pa	508–652	0.1	166–324	2
Thomas#	8	PVT	Liquid	414	0.6–40	0.003(0.01)	220–549	n.a.	258–623	1
Haynes#	12	PVT	Liquid	196	0.6–37	0.01	493–741	0.1	90–300	10(30)
Kratzke#	13	PVT	Liquid	60	2.2–61	n.a.	441–565	n.a.	247–491	10
Straty#	9	PVT	Liquid	59	4.2–35	0.015	250–347	0.1	363–598	n.a.
Goodwin#	14	C_V	Liquid	58	2.1–30	n.a.	495–720	n.a.	100–337	n.a.
Yesavage#	15, 16	C_P	Vapor	7	1.7–6.9	n.a.	26–155	n.a.	339–422	n.a.
Ernst#	17	C_P	Vapor	36	0.05–1.4	n.a.	1–27	n.a.	293–353	0.03%
Yesavage#	15, 16	C_P	Liquid	51	1.7–14	n.a.	268–707	n.a.	339–422	n.a.
Lacam#	18	W	Vapor	50	1.0–13	n.a.	11–209	n.a.	398–498	n.a.
Trusler#	19	W	Vapor	68	0.03–0.07	0.2 kPa	0–16	n.a.	225–375	3
Lacam#	18	W	Liquid	124	1.0–101	n.a.	222–607	n.a.	298–498	n.a.
Younglove#	20	W	Liquid	162	2.0–35	n.a.	496–740	n.a.	90–300	5(30)
Niepmann#	21	W	Liquid	220	2.1–61	n.a.	447–653	n.a.	200–340	n.a.

[a] Data used as input data are denoted by #.
[b] Numerical figures in parentheses denote the maximum experimental uncertainty claimed.

Table II. Experimental Data Along the Saturation Boundary for R-290

First author[a]	Ref.	Property	No. of data	P Range (MPa)	P δP^b (%)	ρ Range ($kg \cdot m^{-3}$)	ρ $\delta\rho$ ($kg \cdot m^{-3}$)	T Range (K)	T δT^b (mK)
Kemp	22	P_S	12	0.0–0.1	n.a.			166–231	n.a.
Reamer	5	P_S	9	1.4–4.1	0.05			313–368	n.a.
Helgeson	23	P_S	16	0.5–3.6	n.a.			278–361	1
Carruth	24	P_S	12	0.0–0.0	0.0312			95–179	0.0328%
Teichmann	25	P_S	15	1.7–3.8	0.02			325–363	10
Kratzke	26	P_S	14	1.3–4.1	0.03			312–368	10
Thomas#	8	P_S	24	0.3–4.2	0.003(0.01)			258–369	1
Reamer	5	ρ''	9			31–151	0.2%	313–368	n.a.
Helgeson	23	ρ''	16			12–106	n.a.	278–361	1
Sliwinski	27	ρ''	15			14–190	0.05	283–369	n.a.
Thomas#	8	ρ''	11			39–173	n.a.	323–369	1
Reamer	5	ρ'	9			329–468	0.2%	313–368	n.a.
Helgeson	23	ρ'	16			342–524	n.a.	278–361	1
Sliwinski	27	ρ'	14			329–514	0.05	283–370	n.a.
Rodosevich	28	ρ'	4			703–727	0.1%	91–115	20
McClune	29	ρ'	17			644–725	0.1%	93–173	100
Haynes	30	ρ'	16			506–719	0.1%	100–289	40
Ely	11	ρ'	18			508–652	0.1%	166–288	2
Orrit#	31	ρ'	31			566–732	0.4	87–244	n.a.
Thomas#	8	ρ'	22			315–547	n.a.	258–369	1
Yesavage#	15, 16	C_σ	28					90–360	n.a.
Goodwin#	14	C_σ	70					86–289	n.a.
Younglove#	20	W'	18					90–290	5(3)
Niepmann#	21	W'	21					200–325	n.a.

[a] Data used for preparing the ancillary correlations regarding the saturation properties are denoted by #.
[b] Numerical figures in parentheses denote the maximum experimental uncertainty claimed.

in Table II. Most of the experimental thermodynamic property data reported prior to 1982 were summarized by Goodwin and Haynes [1], and their reported weighting factors for some sets of experimental data used for the development of their equation of state were useful in the present study. In our work, the temperature values of all experimental data were converted to ITS-90. In the entire fluid phase region, the experimental data cover temperatures from 90 to 623 K, pressures up to 103 MPa, and densities up to 741 $kg \cdot m^{-3}$. It should be noted that we have defined state points with the densities below the critical density, ρ_C, as the vapor phase whereas state points with the densities larger than ρ_C are in the liquid phase.

In general, the selection of input data is one of the most important tasks for the correlator in developing a reliable formulation. In our evaluation of the available measurements, we have paid careful attention with respect to the claimed accuracy, range, number of data points reported, etc., so as to select the input data for modeling as discussed below.

2.2. Ideal-Gas Property Data

For the development of the present formulation for the ideal-gas state contribution, we selected the 19 numerical values (with temperatures from 50 to 1500 K) from the theoretical isobaric heat-capacity values by Chao et al. [32]. The ideal-gas heat capacity correlation proposed by Jaeschke and Schley [33] agrees with the theoretical values by Chao et al. [32] to within $\pm 0.025\%$.

2.3. *PVT* Property Data

We collected more than 2000 experimental *PVT* data points as summarized in Table I. The distribution of the single-phase *PVT* data on a pressure-temperature plane is shown in Fig. 1. Considering the claimed accuracy of each set of measurements and the continuity of these available sets of data, we selected six sets of *PVT* data by Dittmer et al. [10], Ely and Kobayashi [11], Thomas and Harrison [8], Haynes [12], Kratzke and Müller [13], and Straty and Palavra [9] as input data. The two data sets by Thomas and Harrison [8] and Straty and Palavra [9] exist both in the vapor- and liquid-phases as shown in Table I. These sets of data are widely distributed, and the accuracy of these measurements is comparatively good. A set of *PVT* data measured by Warowny et al. [7], which exists in a narrow region near the critical temperature and below the critical density, was only used to compare with the developed formulation. An earlier set of *PVT* data measured by Reamer et al. [5], which covers a wide range of temperatures both in the vapor- and liquid-phases, was not

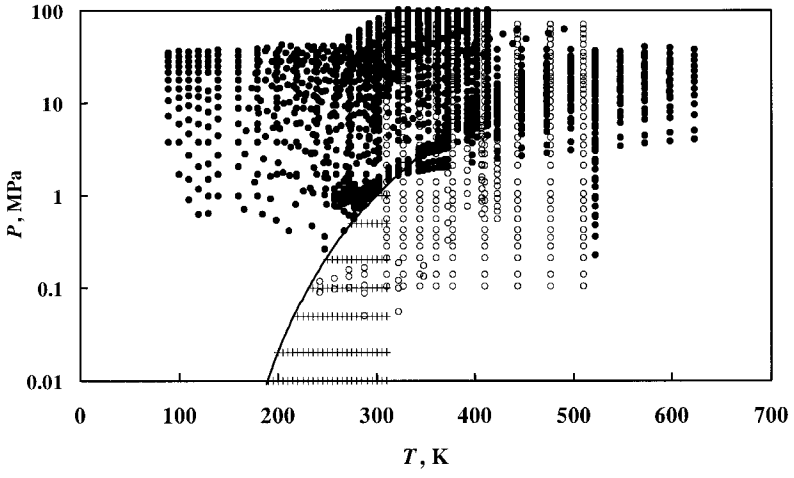

Fig. 1. Distribution of selected *PVT* property data. ● input data, ○ unused data, + supplementary data by the virial equation of state.

selected as input data because of differences from the measured values by Thomas and Harrison [8] in the vapor phase.

2.4. Caloric and Acoustic Property Data

The distribution of the available single-phase caloric and acoustic property data, such as the isochoric and isobaric heat capacities and speeds of sound, is shown on a pressure-temperature plane in Fig. 2, and the data sources are listed in Table I. All of the available heat capacity and speed-of-sound data listed in Table I were used as input data sets. Two sets of essential measurements for these derived thermodynamic properties are available in the vapor phase. The accurate speed-of-sound data measured by Trusler and Zarari [19] are very important as input data, since they are the most recent and one of the most reliable experimental measurements regarding the derived thermodynamic properties of R-290. We also aimed to use the isobaric heat capacity measurements of Ernst and Büsser [17] that cover a limited temperature range in the vapor phase.

Regarding the liquid phase, five sets of derived thermodynamic property data are available. In the range above the critical temperature, only the speed-of-sound data of Lacam [18] are available over the entire pressure range up to 101 MPa, as shown in Fig. 2. At temperatures between 200 and 340 K where the acoustic property data of Niepmann [21] are available, it was observed that measurements of Younglove [20],

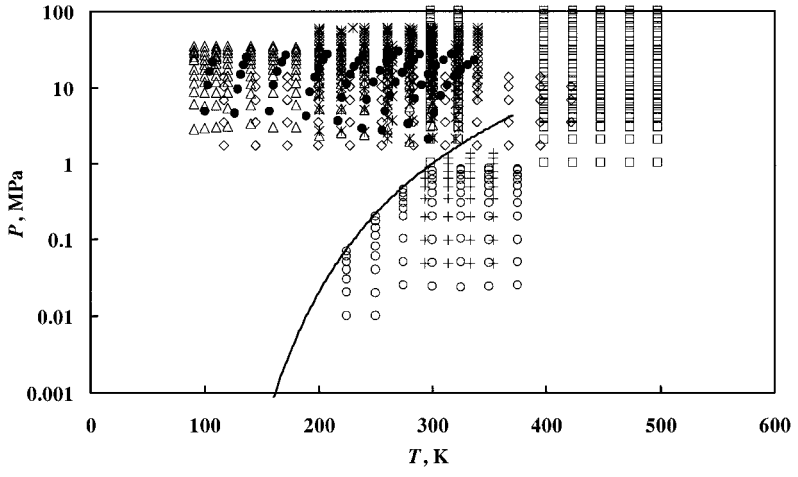

Fig. 2. Distribution of caloric and acoustic property data. ● [C_V] Goodwin [14], ◇ [C_P] Yesavage et al. [15, 16], + [C_P] Ernst and Büsser [17], □ [W] Lacam [18], △ [W] Younglove [20], ⁎ [W] Niepmann [21], ○ [W] Trusler and Zarari [19].

Niepmann [21], and Lacam [18] (the data of Lacam were acquired from Ref. 1 in the present study) agree with each other. A part of the isochoric heat-capacity data of Goodwin [14] that exist in the same temperature range mentioned above is consistent with the observed behavior in the speed-of-sound data of Younglove. At lower temperatures below 200 K, it was not as easy to represent the three sets of data including the isochoric heat-capacity data of Goodwin [14], the isobaric heat-capacity data of Yesavage et al. [15, 16], and the speed-of-sound data of Younglove [20] simultaneously. Because these three different thermodynamic properties are defined by nonlinear relations with each other, it is very difficult to fit all of them accurately by only adjusting the coefficients. Throughout the present modeling, we aimed to improve the consistency of these important properties by a trial-and-error procedure to improve the structure of the formulation.

2.5. Saturation Properties

Many sets of experimental data along the saturation boundary are available in a wide temperature range from the triple point to the critical point, although there exist substantial differences between the experimental data for the vapor-liquid equilibrium properties. In this section, we describe the thermodynamic property information about each saturation property which was used as input data. These input data were also used to develop

the ancillary correlations for the saturated vapor-pressures and saturated vapor- and liquid-densities discussed in the next section.

We collected 102 experimental vapor pressures, P_S, as listed in Table II. As a result of our critical evaluation, we selected 24 P_S measurements by Thomas and Harrison [8] for temperatures above 258 K as a set of input data. These experimental data are thermodynamically consistent with the available experimental PVT data and saturated vapor- and liquid-densities, and the measured accuracy is also sufficient. In the range below atmospheric pressure where the temperature derivatives of P_S have a significant influence on the behavior of the derived thermodynamic properties, we have selected a set of P_S values determined by Magee [34] on the basis of two-phase internal energy measurements by Goodwin [14]. The P_S data of Carruth and Kobayashi [24] at lower temperatures systematically disagree with the Magee data.

We also selected 11 data points by Thomas and Harrison [8] for the saturated vapor densities. For the saturated liquid densities, we selected 31 data points by Orrit and Laupretre [31] and 22 data points by Thomas and Harrison [8]. In the lower temperature region as listed in Table II, the saturated-liquid density measurements by Rodosevich and Miller [28], McClune [29], Haynes and Hiza [30], and Ely and Kobayashi [11] show almost the same behavior as those of Orrit and Laupretre [31].

For the derived thermodynamic properties along the two-phase boundary, the saturated-liquid heat capacity C_σ data by Goodwin [14] behave with the same temperature dependence as those by Yesavage et al. [15, 16] (the data of Yesavage et al. were acquired from Ref. 1). Because the temperature differentials of saturated vapor-pressures relate to saturated-liquid heat capacities which were obtained by adjusting the isochoric heat capacities of the two-phase sample, $C_V^{(2)}$, we aimed to represent the P_S values at lower temperatures determined by Magee [34] as accurately as possible so as to represent the C_σ values of Goodwin [14]. The saturated-liquid speed-of-sound data by Younglove [20], which show the same temperature dependence as those by Niepmann [21], were also useful information for the evaluation of the model along the saturation boundary.

2.6. Ancillary Correlations

A supplementary equation of state for the vapor phase in a limited range of temperatures and pressures and three supplementary correlations for the saturation properties were prepared to generate additional sets of input data for modeling.

For the vapor-phase region at temperatures below 225 K, no thermodynamic property measurements are available. The triple point temperature

of R-290 is extremely low at 85.48 K, and the temperature range where no measurements exist is far broader than that for other conventional refrigerants. In addition, it should be noted that the reliability of any extrapolated values from the model to such a lower temperature region may be decreased significantly. Therefore, we prepared a set of supplementary input PVT data at lower temperatures in the vapor phase which were calculated from the virial equation of state. These 106 supplementary PVT values that cover the temperature range 190 to 310 K with pressures up to 1 MPa are shown in Fig. 1. The virial equation of state has the same functional form as a truncated virial equation of state using the fourth virial coefficient developed by Zhang et al. [35] for HFC refrigerants, as given below.

$$\frac{P}{\rho RT} = 1 + B(T)\,\rho + C(T)\,\rho^2 + D(T)\,\rho^3 \tag{1}$$

where P denotes pressure, T is the temperature, ρ is the density, and R is the gas constant for R-290 with $R = R_m/M$ where the universal gas constant, $R_m = 8.314472\ \mathrm{J \cdot mol^{-1} \cdot K^{-1}}$ [36] and the molar mass, $M = 44.09562\ \mathrm{g \cdot mol^{-1}}$ [37]. The second, $B(T)$, third, $C(T)$, and fourth, $D(T)$ virial coefficients are given by the following expressions:

$$B(T) = b_1 + b_2 \exp(T_r^{-1}) \tag{2}$$

$$C(T) = c_1 + c_2 T_r^{-5} + c_3 T_r^{-12} \tag{3}$$

and

$$D(T) = d_1 T_r^{-2.25} \tag{4}$$

In Eqs. (2)–(4), the reduced temperature $T_r = T/T_C$ is defined with the critical temperature, 369.825 K [8], and the coefficients are $b_1 = 0.2904141$, $b_2 = -0.1972557$, $c_1 = 0.01303094$, $c_2 = 0.00846916$, $c_3 = -0.001790822$, and $d_1 = 0.0002915285$. The present virial equation of state has been developed on the basis of the PVT data by Thomas and Harrison [8] for temperatures between 323 and 369 K and pressures up to 4 MPa. It represents vapor-phase PVT measurements at temperatures between 243 and 369 K and pressures up to 4 MPa reported by Thomas and Harrison [8], Reamer et al. [5], and Dawson and McKetta [6] (the data of Dawson and McKetta were acquired from Ref. 1) within $\pm 0.3\%$ in pressure except in the region near the critical point and the saturation boundary.

Three additional ancillary correlations regarding the saturated vapor-pressures, P_S, and saturated vapor- and liquid-densities, ρ'' and ρ', have

Table III. Coefficients of Eqs. (5)–(7)

i	A_i	B_i	C_i
1	−6.741653	0.5312985	0.2758388
2	1.455497	−1.702073	1.810924
3	−1.312986	−4.998449	−0.8907309
4	−2.111039	−12.18881	0.1273854
5		−42.75035	
6		−107.8777	

also been prepared using the input data mentioned in Section 2.5. It is important to note that these three ancillary correlations were exclusively used to generate complete sets of input data for the saturation properties.

$$\ln \frac{P_S}{P_C} = \frac{1}{1-x}\left(A_1 x + A_2 x^{1.5} + A_3 x^{2.5} + A_4 x^{4.5}\right) \tag{5}$$

$$\ln \frac{\rho''}{\rho_C} = B_1 x^{0.1} + B_2 x^{0.2} + B_3 x^{0.8} + B_4 x^{2.4} + B_5 x^{5.8} + B_6 x^{13.9} \tag{6}$$

$$\ln \frac{\rho'}{\rho_C} = C_1 x^{0.2} + C_2 x^{0.4} + C_3 x^{0.6} + C_4 x^{1.8} \tag{7}$$

Equations (5), (6), and (7) correspond to the saturated vapor-pressure, saturated vapor density, and saturated liquid density, respectively. In each correlation, $x = 1 - T_r$, P_C denotes the critical pressure, 4.24709 MPa, and ρ_C is the critical density, 218.5 $kg \cdot m^{-3}$, as discussed in the next section. The coefficients are listed in Table III. Equation (5) is the Wagner-type vapor-pressure equation which is valid from the triple point temperature to the critical temperature. For the saturated vapor densities at lower temperatures below 278 K where no experimental data are available, we used the calculated density values from Eq. (1) with Eq. (5) for developing Eq. (6). Equations (6) and (7) are also valid for the same temperature range as Eq. (5), i.e., from 85.48 to 369.825 K.

3. EQUATION OF STATE

The dimensionless Helmholtz free energy, $\phi(\tau, \delta)$, model is given by Eq. (8), where the ideal-gas state contribution, $\phi^0(\tau, \delta)$, is expressed by Eq. (9) and the residual real-fluid contribution, $\phi^r(\tau, \delta)$, by Eq. (10). The

independent variables are the inverse reduced temperature, $\tau = T_C/T$, and the reduced density, $\delta = \rho/\rho_C$, while f denotes the Helmholtz free energy.

$$\phi(\tau, \delta) = \frac{f}{RT} = \phi^0(\tau, \delta) + \phi^r(\tau, \delta) \tag{8}$$

$$\phi^0(\tau, \delta) = \ln \delta + a_1^0 + a_2^0 \tau + a_3^0 \ln \tau + \sum_{i=4}^{7} a_i^0 \ln[1 - \exp(-n_i \tau)] \tag{9}$$

$$\phi^r(\tau, \delta) = \sum_{i=1}^{8} a_i \tau^{t_i} \delta^{d_i} + \sum_{i=9}^{13} a_i \tau^{t_i} \delta^{d_i} \exp(-\delta) + \sum_{i=14}^{16} a_i \tau^{t_i} \delta^{d_i} \exp(-\delta^2) + \sum_{i=17}^{19} a_i \tau^{t_i} \delta^{d_i} \exp(-\delta^3) \tag{10}$$

In the present model, the critical temperature $T_C = 369.825$ K and critical density $\rho_C = 218.5\ \text{kg} \cdot \text{m}^{-3}$ determined by Thomas and Harrison [8] are used as reducing parameters. The coefficients of ϕ^0 are listed in Table IV, and the coefficients and exponents of ϕ^r are given in Table V. The other constants used are: the critical pressure, $P_C = 4.24709$ MPa, measured by Thomas and Harrison [8] and the molar gas constant $R = R_m/M$ as described earlier. The resulting critical parameters calculated from the model agree with the data of Thomas and Harrison [8] mentioned above within $\pm 1.8\%$ in density and $\pm 0.2\%$ in pressure.

In Eq. (9), the first term, $\ln \delta$, is related to the ideal-gas law, and the coefficients of a_1^0 and a_2^0 are determined in accord with the reference values of specific enthalpy and specific entropy for the saturated liquid at $T_0 = 273.15$ K, i.e., $h'(T_0) = 200\ \text{kJ} \cdot \text{kg}^{-1}$ and $s'(T_0) = 1.0\ \text{kJ} \cdot \text{kg}^{-1} \cdot \text{K}^{-1}$. With the ideal-gas heat capacity values of Chao et al. [32] as input data mentioned above, the coefficients a_i^0 and n_i of each term were determined by using a nonlinear fitting procedure.

Table IV. Coefficients of Eq. (9)

i	a_i^0	n_i
1	−4.992402	—
2	4.291476	—
3	3.021394	—
4	2.889980	1.048309
5	4.474243	3.053170
6	8.139803	11.42280
7	10.48251	5.042815

Table V. Coefficients and Exponents of Eq. (10)

i	a_i	t_i	d_i
1	2.698378×10^{-1}	−0.25	1
2	-1.339252×10^{0}	1.5	1
3	-2.273858×10^{-2}	−0.75	2
4	2.414973×10^{-1}	0	2
5	-3.321461×10^{-2}	1.25	3
6	2.203323×10^{-3}	1.5	5
7	5.935588×10^{-5}	0.5	8
8	-1.137457×10^{-6}	2.5	8
9	-2.379299×10^{0}	1.5	3
10	2.337373×10^{0}	1.75	3
11	1.242344×10^{-3}	−0.25	8
12	-7.352787×10^{-3}	3	5
13	1.965751×10^{-3}	3	6
14	-1.402666×10^{-1}	4	1
15	-2.093360×10^{-2}	2	5
16	-2.475221×10^{-4}	−1	7
17	-1.482723×10^{-2}	2	2
18	-1.303038×10^{-2}	19	3
19	3.634670×10^{-5}	5	15

To determine the functional form of Eq. (10), we used the regression programs of Tillner-Roth [2] which have proven very effective for the modeling of HFC refrigerants [3, 4]. In this procedure, two algorithms were employed: Wagner's linear stepwise regression analysis for determining the structure including the combination of terms with the aid of statistical parameters regarding the input data, and a nonlinear fitting process for adjusting the coefficients a_i to the data of any thermodynamic properties simultaneously. In the former regression analysis, the "bank of terms" which has been empirically prepared in the present study was used. In the selection process for the essential terms taken from the "bank of terms," we have paid special attention to the following two criteria: (1) to mainain thermodynamic consistency of the model over a very wide range of fluid phase down to 85.48 K, and (2) to keep the same functional structure which will be applied to other hydrocarbons. As a result, we excluded some terms from our preliminary "bank of terms" which unexpectedly influenced the values extrapolated to lower temperatures in the vapor phase. After formulating the preliminary structure of the equation of state by using the linear method mentioned above, the coefficients a_i were nonlinearly refitted and examined for all the input data. Throughout the fitting process, we improved the reproducibility of the model by repeating these two processes.

The equation of state, which contains 19 terms in the residual part, was thus developed on the basis of ITS-90 for the entire fluid phase of R-290. The range of validity of the model covers temperatures from 85.48 K (the triple point temperature) to 623 K, pressures up to 103 MPa, and densities up to 741 $kg \cdot m^{-3}$.

4. COMPARISONS WITH EXPERIMENTAL DATA

4.1. Ideal-Gas State

The ideal-gas part of the equation of state is based on the calculated ideal-gas heat capacity, C_P^0, determined from the spectroscopic data by Chao et al. [32], and the model represents all of the data from 50 to 1500 K within $\pm 0.04\%$. However, the C_P^0 data derived from the isobaric heat capacity measurements by Ernst and Büsser [17] are represented with a maximum relative deviation of $\pm 0.7\%$ and the C_P^0 data derived from the speed-of-sound measurements by Trusler and Zarari [19] are also represented within $\pm 0.5\%$ with systematic deviations shown in Fig. 3. Regarding the systematic deviation of both sets of measured C_P^0 values by Ernst and Büsser [17] and Trusler and Zarari [19], there is still room for discussion concerning the theoretical values of Chao et al. [32] even though the correlations for the ideal-gas heat capacity proposed by Jaeschke and

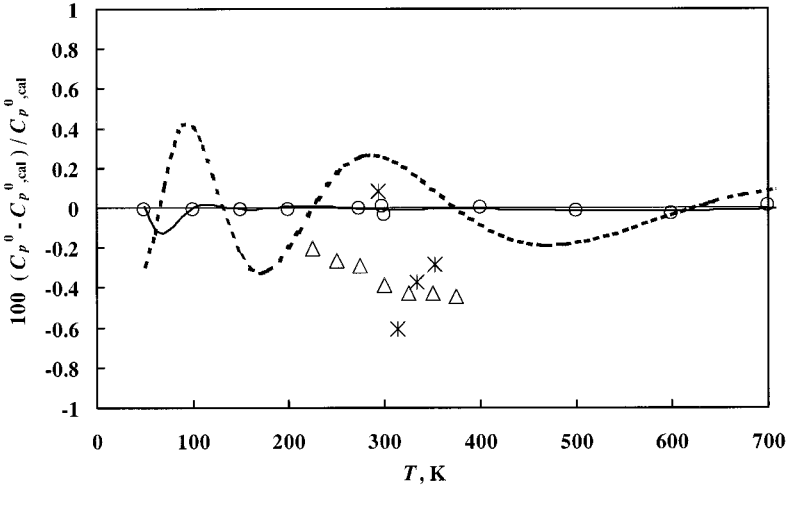

Fig. 3. Deviations of ideal-gas heat capacities C_P^0 from the present model. ○ Chao et al. [32], ✳ Ernst and Büsser [17], △ Trusler and Zarari [19], --- Goodwin and Haynes correlation [1], —— Jaeschke and Schley correlation [33].

Schley [33] and by Goodwin and Haynes [1] also adopted the values by Chao et al. [32] as shown in Fig. 3.

4.2. *PVT* Property Comparison

Pressure deviations for *PVT* property measurements including the selected input and unused data in the vapor phase from the present model are shown in Fig. 4 (for temperatures $T < T_C$) and Fig. 5 ($T > T_C$). In both figures, the most widely distributed *PVT* property data reported by Thomas and Harrison [8] are represented within $\pm 0.4\%$ in pressure; those below the critical temperature are well reproduced within $\pm 0.2\%$ as shown in Fig. 4. At lower temperatures below 310 K in the vapor phase, *PVT* property measurements by Dawson and McKetta [6] are represented within $\pm 0.3\%$ in pressure although they were not used as the input data. In the region above the critical temperature, as shown in Fig. 5, the data of Straty and Palavra [9] are reasonably represented within $\pm 0.4\%$ in pressure, whereas the data of Warowny et al. [7] are represented within $\pm 0.5\%$ in pressure except for two data points above 165 $kg \cdot m^{-3}$.

The density deviations of the liquid phase data are shown in Fig. 6. The accurate *PVT* measurements in the liquid phase by Ely and Kobayashi [11], Haynes [12], and Kratzke and Müller [13] are well represented within $\pm 0.3\%$ in density. Most of the data measured by Thomas and

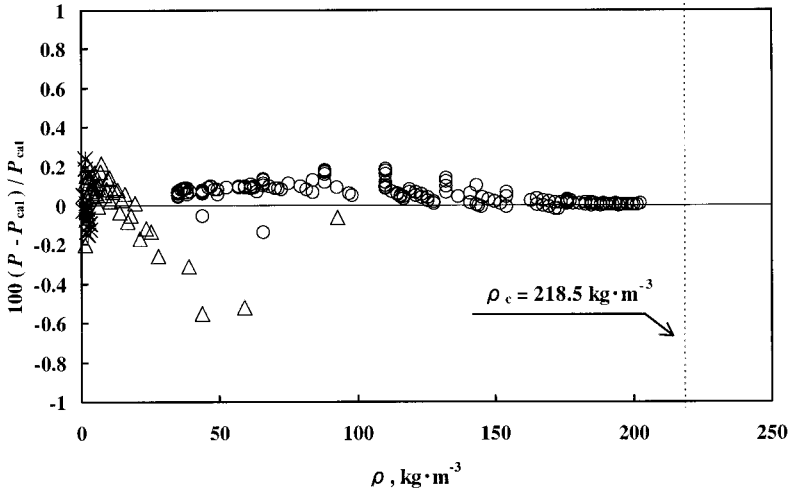

Fig. 4. Pressure deviations of *PVT* data from Eq. (8) for temperatures below T_C in the vapor phase. △ Reamer et al. [5], ∗ Dawson and McKetta [6], ○ Thomas and Harrison [8].

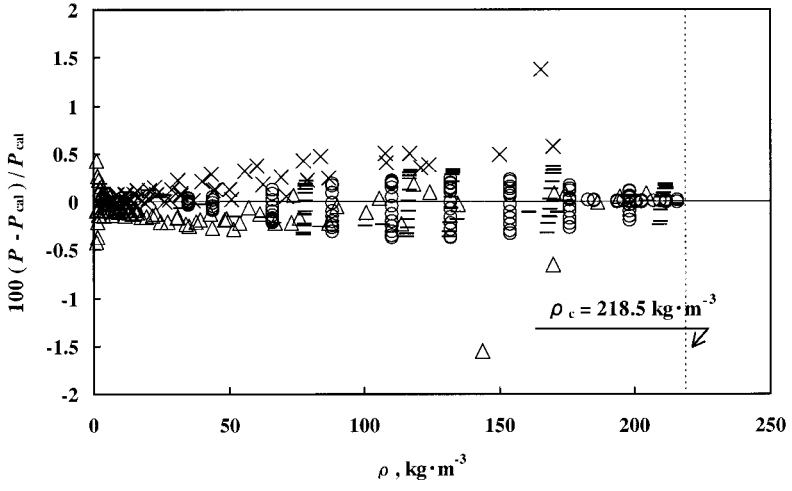

Fig. 5. Pressure deviations of *PVT* data from Eq. (8) for temperatures above T_C in the vapor phase. △ Reamer et al. [5], × Warowny et al. [7], ○ Thomas and Harrison [8], — Straty and Palavra [9].

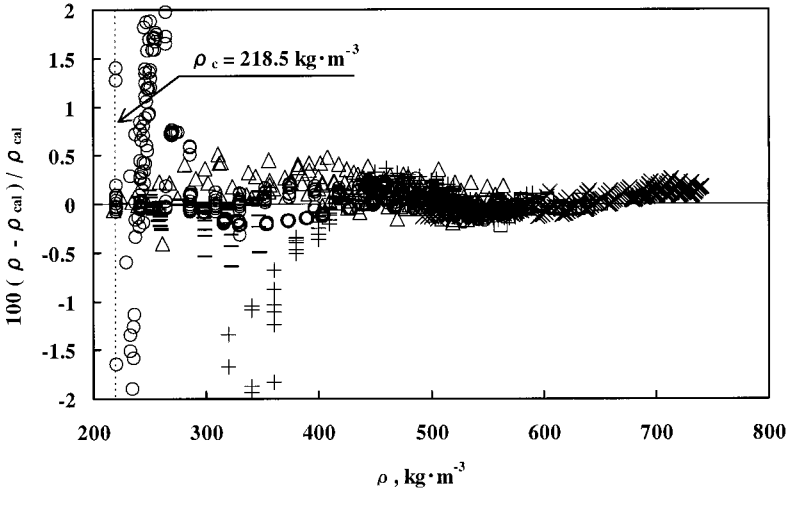

Fig. 6. Density deviations of *PVT* measurements from Eq. (8). △ Reamer et al. [5], + Dittmer et al. [10], □ Ely and Kobayashi [11], ○ Thomas and Harrison [8], × Haynes [12], ◇ Kratzke and Müller [13], — Straty and Palavra [9].

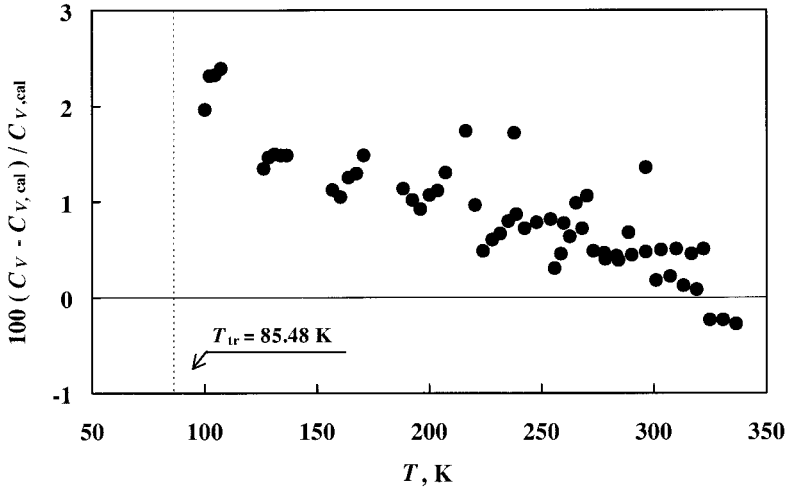

Fig. 7. Deviations of the isochoric heat capacity data from Eq. (8). ● Goodwin [14].

Harrison [8] and Straty and Palavra [9], which include a large number of measurements in the critical region and near the saturation boundary, are also represented within $\pm 0.5\%$ except for a considerable number of data points near the critical point. The input data by Dittmer et al. [10] including those under high pressures up to 103 MPa are mostly reproduced

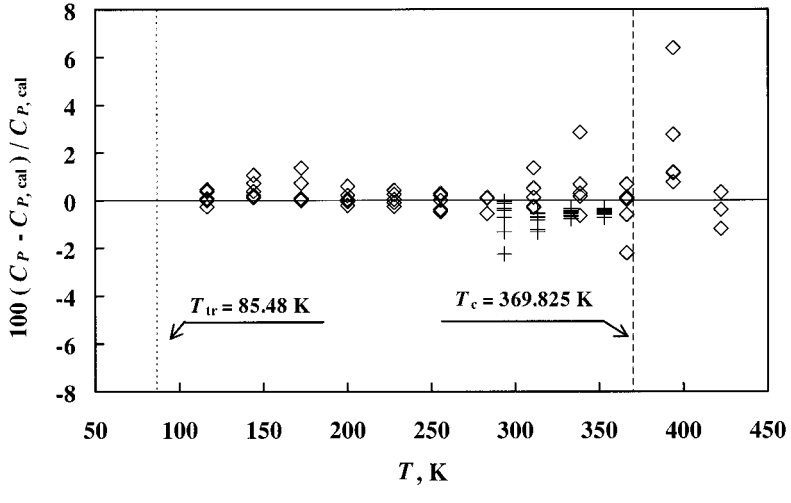

Fig. 8. Deviations of the isobaric heat capacity data from Eq. (8). ◇ Yesavage et al. [15, 16], + Ernst and Büsser [17].

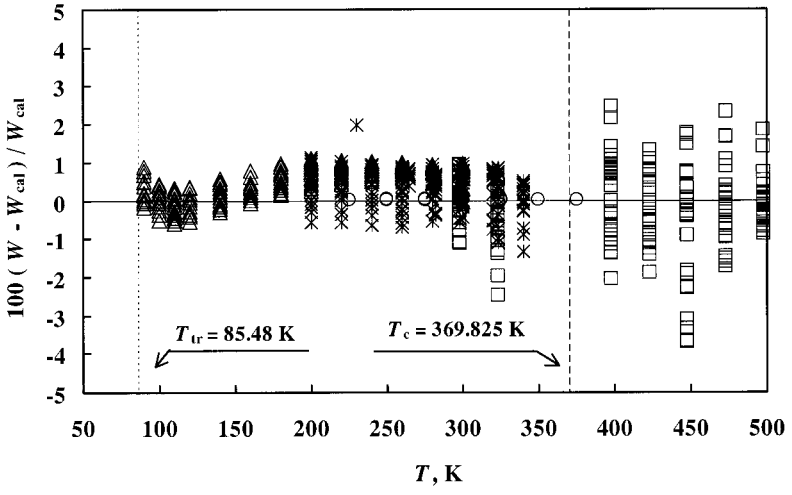

Fig. 9. Deviations of the speed-of-sound data from Eq. (8). □ Lacam [18], △ Younglove [20], ∗ Niepmann [21], ○ Trusler and Zarari [19].

within ±0.5%, except for several data points below 380 $kg \cdot m^{-3}$, while the unused data of Reamer et al. [5] deviate by about ±0.5%.

4.3. Caloric and Acoustic Property Comparison

Comparisons of the present model with reported experimental data for the isochoric heat capacity, C_V, isobaric heat capacity, C_P, and speed of sound, W, are shown in Figs. 7 through 9.

A series of C_V measurements by Goodwin [14] in the liquid phase is well reproduced within the claimed uncertainty of ±2.0% as shown in Fig. 7 except for three data points near 100 K. In the vapor phase, the C_P measurements of Ernst and Büsser [17] shown in Fig. 8 are represented within 0.9% except for four data points near the saturation boundary. At lower temperatures below 200 K, the C_P data of Yesavage et al. [15, 16] are reasonably reproduced within ±1.4%, while their data at higher temperatures give somewhat more scattered deviations. The most recent and highly accurate speed-of-sound measurements by Trusler and Zarari [19] in the vapor phase are well represented within ±0.06% as shown in Fig. 9. In the liquid phase below the critical temperature, the speed-of-sound data of Younglove [20] are represented within ±1.1%, whereas the speed-of-sound data of Niepmann [21] agree with the present model within ±1.4% except for a single data point at 230 K. The data of Lacam [18] at higher pressures from 60 to 101 MPa are represented within ±1.2%,

although those at lower pressures below 40 MPa show a slightly larger deviation.

4.4. Saturation-Property Comparison

For comparisons of P_S measurements with the present model, Fig. 10 shows a relative deviation together with an absolute deviation of ± 1 kPa. The most accurate P_S measurements by Thomas and Harrison [8] at temperatures above 258 K are well represented by the model within $\pm 0.05\%$. At lower temperatures below 230 K, the calculated P_S values by Magee [34] agree with the equation of state within about ± 50 Pa, whereas the data by Kemp and Egan [22] exhibit lower P_S values. At the triple point temperature, the calculated P_S value by Magee [34] is represented within 2.2% corresponding to an absolute deviation of 5.0 μPa. Four other sets of P_S data by Reamer et al. [5], Helgeson and Sage [23], Teichmann [25], and Kratzke [26] at higher temperatures show significant deviations as clearly seen in Fig. 10.

Comparisons of the saturated vapor- and liquid-densities are shown in Figs. 11 and 12, respectively. The saturated vapor- and liquid-density measurements by Thomas and Harrison [8] at temperatures above 258 K

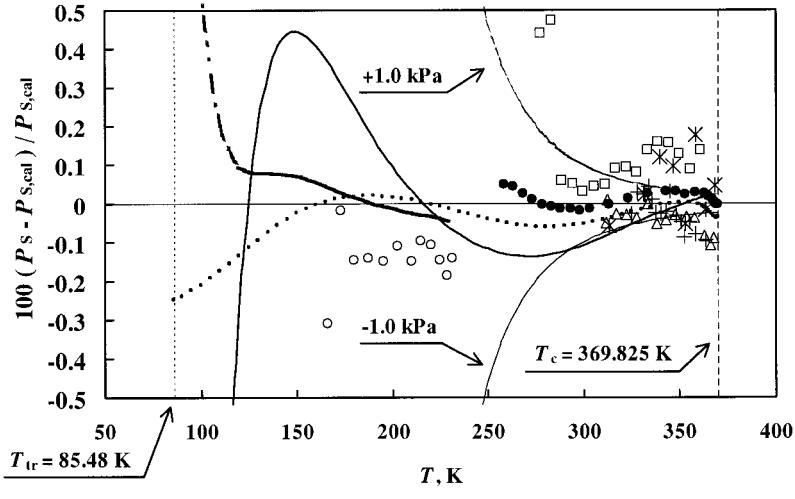

Fig. 10. Deviations of measured and calculated vapor pressure values from the present model. ○ Kemp and Egan [22], ⁎ Reamer et al. [5], □ Helgeson and Sage [23], + Teichmann [25], △ Kratzke [26], ● Thomas and Harrison [8], –·– calculation by Magee [34], ··· REFPROP Ver. 6.01 (Younglove and Ely model [38]), — Span and Wagner model [39].

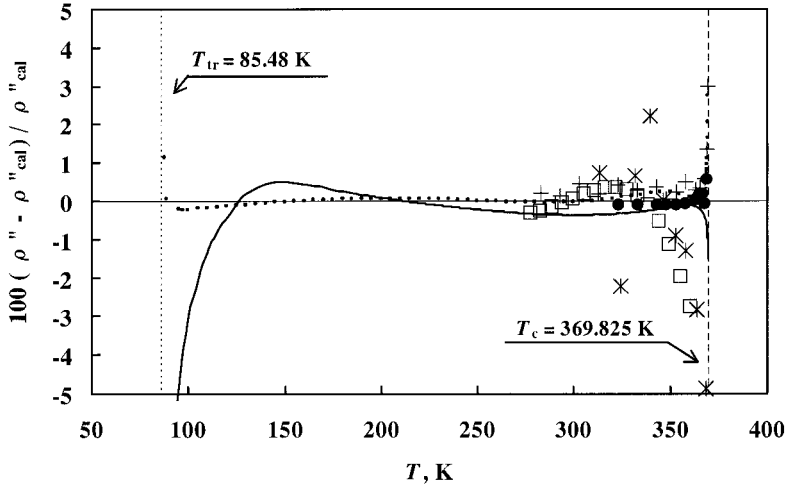

Fig. 11. Deviations of measured saturated-vapor densities ρ'' from the present model. ⁎ Reamer et al. [5], □ Helgeson and Sage [23], + Sliwinski [27], ● Thomas and Harrison [8], ··· REFPROP Ver. 6.01 (Younglove and Ely model [38]), — Span and Wagner model [39].

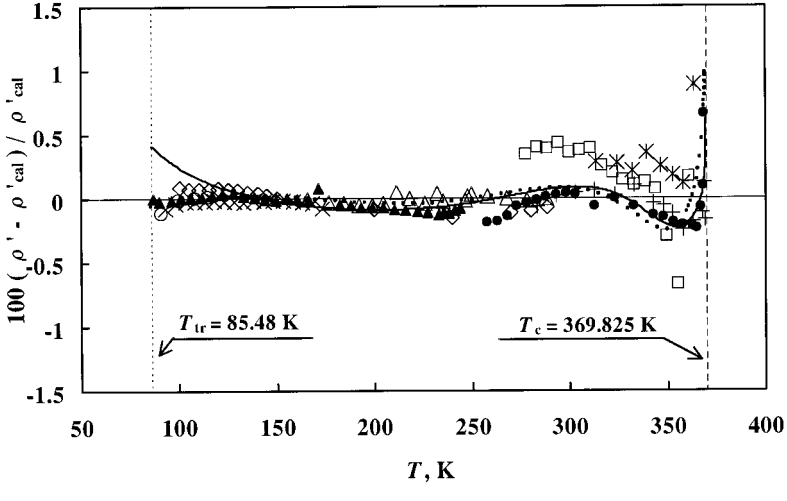

Fig. 12. Deviations of measured saturated-liquid densities ρ' from the present model. ⁎ Reamer et al. [5], □ Helgeson and Sage [23], + Sliwinski [27], ○ Rodosevich and Miller [28], × McClune [29], ◇ Haynes and Hiza [30], △ Ely and Kobayashi [11], ▲ Orrit and Laupretre [31], ● Thomas and Harrison [8], ··· REFPROP Ver. 6.01 (Younglove and Ely model [38]), — Span and Wagner model [39].

are well represented by the present model within ± 0.2 and $\pm 0.3\%$, respectively, except for a single data point for both the vapor- and liquid-phase near the critical temperature. At this highest temperature, 369.125 K, the deviation of the saturated density data of Thomas and Harrison [8] reach 0.7%. In the temperature range where the data of Thomas and Harrison [8] are available, as shown in Figs. 11 and 12, significant deviations of saturated vapor- and liquid-density data by Reamer et al. [5] and Helgeson and Sage [23] can be observed, whereas the saturation density data in both phases by Sliwinski [27] behave similarly to those of Thomas and Harrison [8]. At lower temperatures, the saturated-liquid density data by Orrit and Laupretre [31] are well represented within $\pm 0.2\%$, whereas four other sets of saturated liquid-density data by Rodosevich and Miller [28], McClune [29], Haynes and Hiza [30], and Ely and Kobayashi [11] are also reproduced satisfactorily.

The relative deviations with respect to the derived thermodynamic properties at saturation are shown in Fig. 13. The saturated-liquid heat capacity C_σ data by Goodwin [14] are well represented by the present model within $\pm 0.8\%$, while the C_σ data by Yesavage et al. [15, 16] are reproduced within $\pm 1.1\%$. The saturated-liquid speed-of-sound data of Younglove [20] and Niepmann [21] show systematic deviations depending on temperatures, but they are both represented within $\pm 1.1\%$ over the entire temperature range. The comparisons mentioned above show that the

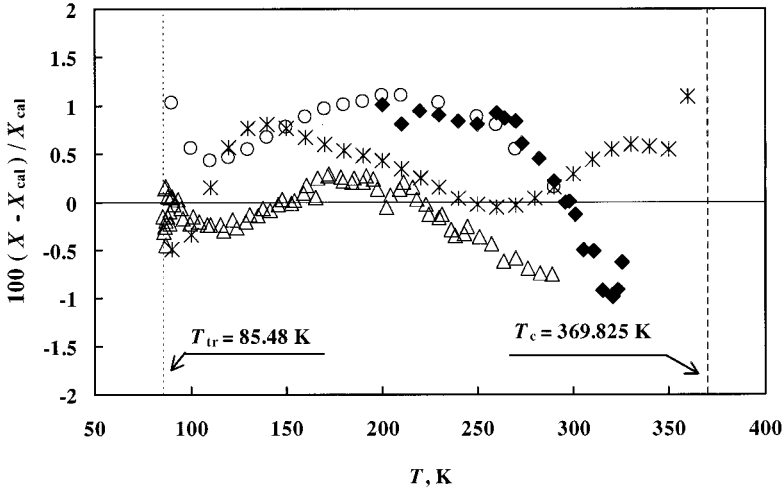

Fig. 13. Deviations of the saturated-liquid heat capacity and speed-of-sound data from Eq. (8). ✳ [C_σ] Yesavage et al. [15, 16], △ [C_σ] Goodwin [14], ○ [W'] Younglove [20], ◆ [W'] Niepmann [21].

present formulation can reproduce the thermodynamic properties along the saturation boundary of R-290 reasonably well over the entire range of temperatures from the triple point to the critical point.

4.5. Behavior of the Derived Thermodynamic Properties

As one of the most important tests for the accuracy of the thermodynamic model, the behavior of C_V, C_P, W, and the Joule–Thomson coefficients, μ, over an extended range of temperatures and pressures are shown in Figs. 14 through 17, respectively. These derived thermodynamic properties were calculated along the isobars at 1, 2, 3, 4, 5, 6, 10, 20, 50, and 100 MPa for temperatures extending up to 650 K in order to examine the extrapolated behavior of the model. The ideal-gas heat capacities calculated from the model are also included in Figs. 14 and 15.

As shown in Figs. 14 and 15, the calculated C_V and C_P values along different isobars behave very smoothly and they exhibit physically sound behavior over the range of interest. There are no intersecting isobars, although the isobars at 50 and 100 MPa near the triple point where no experimental data are available show a slightly unrealistic behavior. Figures 16 and 17 illustrate similar behavior for W and μ along different isobars. The isobars for W are physically correct over the entire fluid phase, but the μ behavior at higher pressures near the triple point temperature exhibit some minor intersections among the isobars.

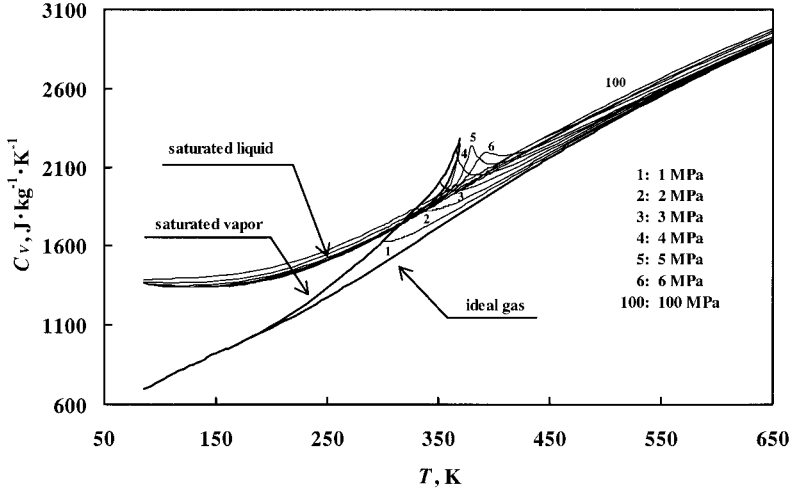

Fig. 14. Calculated isochoric heat capacity values along isobars using the present model.

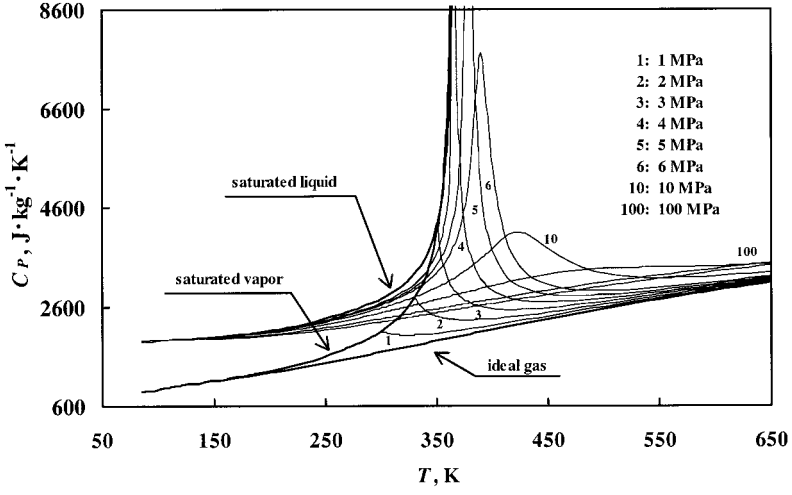

Fig. 15. Calculated isobaric heat capacity values along isobars using the present model.

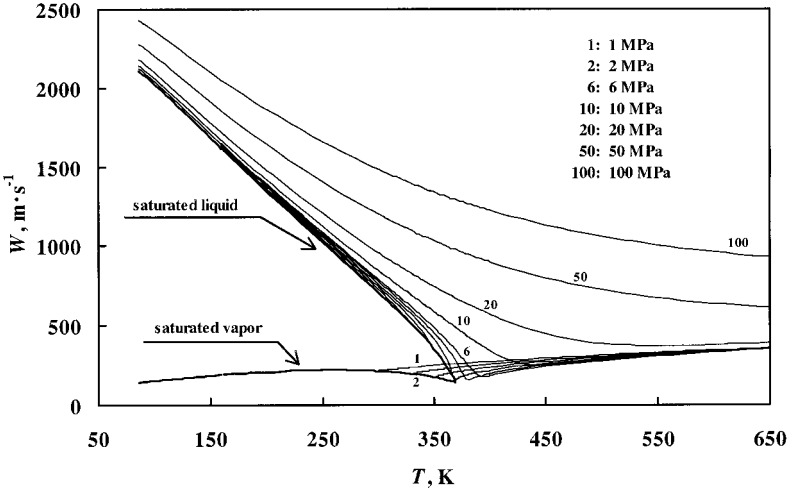

Fig. 16. Calculated speed-of-sound values along isobars using the present model.

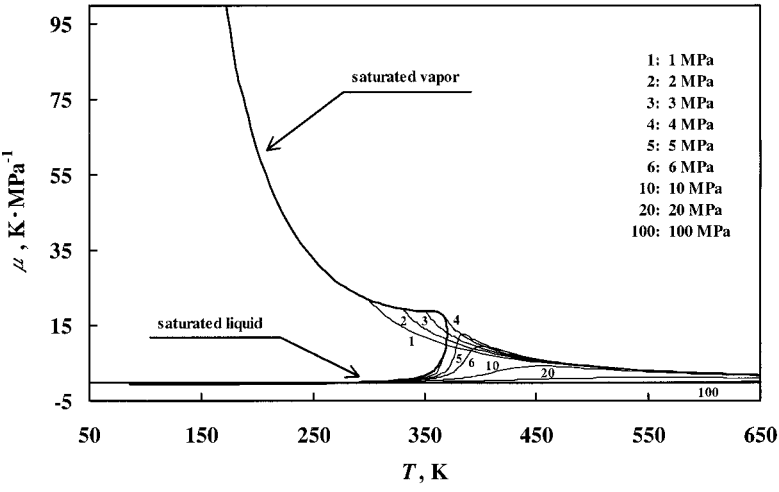

Fig. 17. Calculated Joule–Thomson coefficient values along isobars using the present model.

5. COMPARISON WITH EXISTING MODELS

One of the earliest thermodynamic property models that covers the entire fluid phase of R-290 was developed by Goodwin and Haynes [1] who also summarized and evaluated most of the available experimental data published prior to 1982. Their model, however, consists of a single equation of state that covers the entire fluid phase and several other associated correlations with respect to vapor pressure and saturated vapor- and liquid-densities. We did not compare the present model with their model, since we found that their model was too complex and calculated C_P values in the critical region did not exhibit physically sound behavior. Instead, we compare the present model with two other representative models, i.e., those by Younglove and Ely [38] and Span and Wagner [39], so as to confirm its reliability with the aid of graphical and statistical examinations.

The model developed by Younglove and Ely [38] is a modified BWR equation of state with 32 coefficients. Its range of validity covers temperatures up to 600 K and pressures up to 100 MPa. Its high reproducibility regarding the available thermodynamic property measurements are confirmed in the fluid phase of R-290, especially in the liquid phase and at the saturation boundary, and this model is currently adopted in the software package, REFPROP (Ver. 6.01), published by NIST [40]. We used subroutines given in the source program of REFPROP (Ver. 6.01) for comparing the

Younglove and Ely model with experimental data. For precise comparison, the temperature scale of the Younglove and Ely model was converted from IPTS-68 to ITS-90.

The other model with which we compared is a Helmholtz free energy equation of state developed by Span and Wagner [39]. This equation of state has excellent reproducibility in the vapor phase, and the total number of terms for the residual part is only 12. It is also important to note that Span and Wagner are applying the same combination of terms with that model to 15 different substances.

The comparisons of essential thermodynamic properties along the saturation boundary with the present model are shown in Figs. 10 through 12. For the saturated vapor-pressure, P_S, the most accurate experimental data by Thomas and Harrison [8] are better represented by the present formulation than the other two models, as shown in Fig. 10. At extremely low temperatures below the normal boiling point, it is observed that the present model has the most appropriate representation of the calculated P_S values by Magee [34]. In addition, the reasonable representations of the saturated vapor- and liquid-densities by the present model are also confirmed among different models as depicted in Figs. 11 and 12, respectively.

The accuracy and reliability of each model in the single phase region were examined statistically in terms of the absolute average deviation "AAD," the bias "BIAS," the standard deviation "SDV," the root-mean-square deviation "RMS," and the maximum percentage deviation "MAX%" with respect to each data set as summarized in Table VI. The PVT data of Thomas and Harrison [8] and Dittmer et al. [10], and the W data of Lacam [18] for temperatures above 600 K and pressures above 100 MPa have been compared with the Younglove and Ely model [38], although that model is valid only up to 600 K and 100 MPa.

The statistical values in Table VI show that the present equation of state satisfactorily reproduces the PVT data better than the other two models. In the vapor-phase region, the numerical differences among the statistical results including AAD, BIAS, SDV, and RMS are less than $\pm 0.08\%$ between our model and the other two models. As for the liquid-phase PVT data, except those in the region near the critical point, the differences of the above-mentioned statistical values are nearly zero. The present model represents the experimental data in the liquid phase of Thomas and Harrison [8] and Straty and Palavra [9] that include a large amount of PVT data near the critical point better than the other models as observed in Table VI.

Statistical comparisons of caloric and acoustic property data with all the models are presented in Table VI. In the vapor-phase region, the speed-of-sound data by Trusler and Zarari [19] are better represented by the

Table VI. Statistical Comparison of Three Models with Single-Phase Experimental Data[a]

Property	Phase[b]	No. of Data	First author	Present model					Younglove and Ely model (REFPROP Ver. 6.01)					Span and Wagner model				
				AAD	BIAS	SDV	RMS	MAX%	AAD	BIAS	SDV	RMS	MAX%	AAD	BIAS	SDV	RMS	MAX%
PVT	V1	47	Reamer [5]	0.12	0.00	0.16	0.16	−0.55	0.11	0.04	0.14	0.14	−0.42	0.12	−0.03	0.18	0.18	−0.63
PVT	V2	92	Reamer [5]	0.15	−0.09	0.21	0.23	−1.56	0.12	−0.06	0.22	0.23	−1.67	0.15	−0.11	0.22	0.24	−1.64
PVT	V1	18	Dawson [6]	0.10	−0.01	0.12	0.12	0.24	0.09	0.01	0.12	0.11	0.25	0.10	−0.02	0.12	0.12	0.23
PVT	V2	51	Warowny [7]	0.19	0.18	0.24	0.30	1.38	0.24	0.23	0.23	0.33	1.42	0.15	0.14	0.18	0.23	1.07
PVT	V1	167	Thomas [8]	0.05	0.05	0.05	0.07	0.18	0.11	0.10	0.08	0.13	0.26	0.03	0.00	0.04	0.04	−0.21
PVT	V2	155	Thomas [8]	0.10	−0.03	0.14	0.14	−0.38	0.11	0.03	0.13	0.14	0.34	0.06	−0.04	0.08	0.09	−0.26
PVT	V2	85	Straty [9]	0.17	0.00	0.20	0.20	−0.38	0.17	0.05	0.21	0.21	0.54	0.11	−0.04	0.12	0.13	−0.26
PVT	L	167	Reamer [5]	0.16	0.12	0.15	0.20	0.51	0.18	0.14	0.20	0.24	1.09	0.15	0.11	0.17	0.20	0.60
PVT	L	336	Dittmer [10]	0.21	−0.05	0.45	0.45	−3.74	0.18	−0.01	0.40	0.40	−3.31	0.18	−0.05	0.42	0.43	−3.59
PVT	L	222	Ely [11]	0.03	−0.01	0.03	0.04	−0.23	0.03	0.02	0.04	0.05	−0.15	0.04	0.03	0.04	0.05	−0.18
PVT	L	414	Thomas [8]	0.54	0.19	1.43	1.44	13.23	0.82	0.71	2.00	2.12	14.59	0.51	−0.22	1.40	1.41	10.27
PVT	L	196	Haynes [12]	0.10	0.02	0.11	0.11	0.26	0.10	0.04	0.12	0.13	0.28	0.09	−0.01	0.11	0.11	−0.28
PVT	L	60	Kratzke [13]	0.13	0.08	0.12	0.15	0.24	0.11	0.08	0.10	0.13	0.21	0.10	0.06	0.10	0.11	0.20
PVT	L	59	Straty [9]	0.13	−0.10	0.16	0.19	−0.65	0.15	−0.07	0.18	0.19	−0.42	0.16	−0.13	0.17	0.22	−0.59
C_V	L	58	Goodwin [14]	0.90	0.87	0.61	1.06	2.38	0.93	0.88	0.64	1.08	2.20	1.31	0.10	2.01	1.99	−7.55
C_P	V	7	Yesavage [15, 16]	0.99	−0.44	1.14	1.14	−2.20	1.11	−0.50	1.15	1.17	−1.86	0.93	−0.25	1.21	1.15	−2.25
C_P	V	36	Ernst [17]	0.62	−0.62	0.39	0.73	−2.25	0.88	−0.88	0.31	0.93	−1.53	0.45	−0.45	0.16	0.48	−0.91
C_P	L	51	Yesavage [15, 16]	0.56	0.45	1.07	1.15	6.38	0.56	0.41	1.19	1.24	7.44	1.28	−0.29	2.27	2.27	7.39
W	V	50	Lacam [18]	1.13	−1.06	1.00	1.45	−3.69	1.16	−1.05	1.05	1.48	−3.74	1.13	−1.06	0.99	1.45	−3.66
W	V	68	Trusler [19]	0.02	0.02	0.01	0.02	0.05	0.05	0.05	0.03	0.06	0.16	0.01	0.01	0.01	0.01	−0.03
W	L	124	Lacam [18]	0.65	0.21	0.83	0.85	−2.49	0.64	0.27	0.86	0.90	4.19	0.55	0.17	0.74	0.75	2.54
W	L	162	Younglove [20]	0.55	0.46	0.44	0.64	1.09	0.30	−0.07	0.35	0.36	−0.88	0.54	0.24	0.57	0.62	−1.42
W	L	220	Niepmann [21]	0.52	0.34	0.50	0.60	1.99	0.37	−0.27	0.38	0.46	1.97	0.31	0.09	0.40	0.41	2.26

[a] Note that deviations of *PVT* data are given with respect to densities in the liquid phase, whereas pressures in the vapor phase.
[b] V1 denotes the vapor phase at temperatures $T < T_C$, while V2, at temperatures $T > T_C$.

present model and the Span and Wagner model [39] than by the Younglove and Ely model [38] which was developed without using these data. The Span and Wagner model [39] shows a slightly better representation for the isobaric heat capacity. More precisely, the difference in the reproducibility between the Span and Wagner model and the present model exists only for the isobaric heat-capacity data by Ernst and Büsser [17], particularly for the data near the saturation boundary. We believe therefore, that the present model exhibits an almost equivalent representation similar to the Span and Wagner model.

Regarding the liquid phase, the C_V measurements of Goodwin [14] and the C_P measurements of Yesavage et al. [15, 16] are represented with the highest reproducibility by the present model. Table VI also shows that the best agreement of the model of Younglove and Ely [38] is given for the W data of Younglove [20], while that of the Span and Wagner model [39] for the W data of Niepmann [21]. However, the differences among statistical values calculated from the three different models are not very significant, in general. From the above-mentioned comparisons, it is reasonable to conclude that the present model also does a good job representing the reliable sets of caloric and acoustic property data in the liquid phase.

6. CONCLUSION

We developed a fundamental equation of state to cover the entire fluid phase of propane (R-290) with 19 terms in the residual part. In our model, selected input data for PVT, caloric, acoustic, and saturation properties were used simultaneously in the optimization process. In addition, we used four sets of supplementary input data generated from a virial equation of state valid in a limited vapor-phase region and additional ancillary correlations for saturated vapor-pressures and saturated vapor- and liquid-densities. Throughout the modeling effort, we ensured that the equation represented the thermodynamic properties of R-290 as accurately as possible to cover a wide range of temperatures from the triple point temperature (85.48 K) to 623 K, since this triple point temperature is extremely low in the case of R-290 among simple hydrocarbons.

We have provided a series of detailed comparisons of the developed model with the available experimental data including both selected input data and unused data reported for various thermodynamic properties. A systematic examination of the calculated values for several derived thermodynamic properties such as the isochoric and isobaric heat capacities, speeds of sound, and Joule–Thomson coefficients has also been conducted in terms of graphical confirmation of the calculated property values along different isobars.

In addition, we have also discussed the reliability of other models proposed by Younglove and Ely and by Span and Wagner in comparison with the present model. A statistical analysis has been extensively applied among the three models. The present model showed excellent thermodynamic consistency in representing the thermodynamic properties over the entire fluid phase of R-290 at temperatures up to 623 K and pressures up to 103 MPa with a relatively short dimensionless Helmholtz free energy function.

ACKNOWLEDGMENTS

The authors wish to express gratitude to Dr. R. Tillner-Roth who developed the original source programs for the optimization procedure. We are also grateful to Dr. J. W. Magee and Prof. W. Wagner who kindly provided their unpublished data and models. A valuable set of information about earlier experimental data was kindly provided by Dr. W. M. Haynes. Valuable discussions and suggestions by Drs. A. Yokozeki, J. Li, and Prof. H. Sato are highly appreciated.

REFERENCES

1. R. D. Goodwin and W. M. Haynes, *Thermophysical Properties of Propane from 85 to 700 K at Pressures to 70 MPa*, NBS Monograph, Vol. 170 (U.S. Department of Commerce, Washington, DC, 1982).
2. R. Tillner-Roth, several programs for the modeling were provided as private communication (1996).
3. R. Tillner-Roth and A. Yokozeki, *J. Phys. Chem. Ref. Data* **26**:1273 (1997).
4. R. Tillner-Roth, J. Li, A. Yokozeki, H. Sato, and K. Watanabe, *Thermodynamic Properties of Pure and Blended Hydrofluorocarbon (HFC) Refrigerants* (Jpn. Soc. Refrig. Air Cond. Engrs., Tokyo, 1998).
5. H. H. Reamer, B. H. Sage, and W. N. Lacey, *Ind. Eng. Chem.* **41**:482 (1949).
6. P. P. Dawson and J. J. McKetta, *Petroleum Refiner* **39**:151 (1960).
7. W. Warowny, P. Wielopolski, and J. Stecki, *Physica* **91A**:73 (1978).
8. R. H. P. Thomas and R. H. Harrison, *J. Chem. Eng. Data* **27**:1 (1982).
9. G. C. Straty and A. M. F. Palavra, *J. Res. Natl. Bur. Stand.* **89**:375 (1984).
10. P. Dittmer, F. Schulz, and G. Strese, *Chemie-Ing.-Techn.* **34**:437 (1962).
11. J. F. Ely and R. Kobayashi, *J. Chem. Eng. Data* **23**:221 (1978).
12. W. M. Haynes, *J. Chem. Thermodyn.* **15**:419 (1983).
13. H. Kratzke and S. Müller, *J. Chem. Thermodyn.* **16**:1157 (1984).
14. R. D. Goodwin, *J. Res. Natl. Bur. Stand.* **83**:440 (1978).
15. V. F. Yesavage, D. L. Katz, and J. E. Powers, *J. Chem. Eng. Data* **14**:197 (1969).
16. V. F. Yesavage, Ph.D. dissertation (University of Michigan, Ann Arbor, 1968).
17. G. Ernst and J. Büsser, *J. Chem. Thermodyn.* **2**:787 (1970).
18. A. Lacam, *J. Rech. Centre Natl. Rech. Sci. Lab. Bellevue* **34**:25 (1956).
19. J. P. M. Trusler and M. P. Zarari, *J. Chem. Thermodyn.* **28**:329 (1996).

20. B. A. Younglove, *J. Res. Natl. Bur. Stand.* **86**:165 (1981).
21. R. Niepmann, *J. Chem. Thermodyn.* **16**:851 (1984).
22. J. D. Kemp and C. J. Egan, *J. Am. Chem. Soc.* **60**:1521 (1938).
23. N. L. Helgeson and B. H. Sage, *J. Chem. Eng. Data* **12**:47 (1967).
24. G. F. Carruth and R. Kobayashi, *J. Chem. Eng. Data* **18**:115 (1973).
25. J. Teichmann, Ph.D. dissertation (Ruhr University, Bochum, 1978).
26. H. Kratzke, *J. Chem. Thermodyn.* **12**:305 (1980).
27. P. Sliwinski, *Z. Phys. Chem. Neue Folge* **63**:263 (1969).
28. J. B. Rodosevich and R. C. Miller, *AIChE J.* **19**:729 (1973).
29. C. R. McClune, *Cryogenics* **16**:289 (1976).
30. W. M. Haynes and M. J. Hiza, *J. Chem. Thermodyn.* **9**:179 (1977).
31. J. E. Orrit and J. M. Laupretre, *Adv. Cryog. Eng.* **23**:573 (1978).
32. J. Chao, R. C. Wilhoit, and B. J. Zwolinski, *J. Phys. Chem. Ref. Data* **2**:427 (1973).
33. M. Jaeschke and P. Schley, *Int. J. Thermophys.* **16**:1381 (1995).
34. J. W. Magee, new information for the saturation vapor-pressure of lower temperatures was provided as a private communication (1999).
35. H.-L. Zhang, H. Sato, and K. Watanabe, *J. Chem. Eng. Data* **41**:1401 (1996).
36. P. J. Mohr and B. N. Taylor, *J. Phys. Chem. Ref. Data* **28**:1713 (1999).
37. T. B. Coplen, *J. Phys. Chem. Ref. Data* **26**:1239 (1997).
38. B. A. Younglove and J. F. Ely, *J. Phys. Chem. Ref. Data* **16**:577 (1987).
39. R. Span and W. Wagner, submitted to *Int. J. Thermophys.* (2000).
40. M. O. McLinden, S. A. Klein, E. W. Lemmon, and A. P. Peskin, *NIST Thermodynamic and Transport Properties of Refrigerants and Refrigerant Mixtures (REFPROP)* Ver. 6.01 (U.S. Department of Commerce, Washington, DC, 1998).